MONABIPHOT

Master Thesis

Nestor, Gisbert Quilis
nesgisqui@gmail.com

Title of the research Project:
Preparation of plasmonic nanostructures for biosensors applications

HOST INSTITUTION

Austrian Institute of Technology (AIT) GmbH - Donau-City-Straße 1 | 1220 Vienna | Austria

BioSensor Technologies, Dostalek Plasmonic Biosensor Group
http://www.ait.ac.at/ http://www.jakubdostalek.cz/

ADVISERS:

Professor or *lab director*
Name: Dostalek **First name:** Jakub
E-mail address: jakub.dostalek@ait.ac.at

Defence date: 22/ 07/2015

Acknowledgments

I would like to express my gratitude to my group leader, Dr. Jakub Dostalek, for his acceptance, guidance and great ideas that enable me to complete this thesis. I would also like to thank the Austrian Institute of Techonology (AIT) for the contract and research facilities provided.

I want to convey a great thanks to Imran Khan, his support and help for the laser interference lithography has been invaluable.

I would like to acknowledge the MONABIPHOT consortium for the acceptance and the Erasmus Mundus Joint Master Degrees (EMJMDs) programme for the funding. Special thanks to Prof. Isabelle Ledoux-Rak, for organizing constantly all the masters programme.

I would like to express thanks to my colleagues at the AIT, for the nice and friendly atmosphere created in the lab every single day.

For any errors or inadequacies that may remain in this work, of course, the responsibility is entirely mine.

Abstract

Plasmonic nanostructures exhibit unique optical properties that can be tailored in order to efficiently amplify sensitivity in various optical spectroscopy techniques used for the analysis of biomolecules. Among others, the plasmonic amplification of fluorescence bioassays was demonstrated to advance their sensitivity by several orders of magnitude and thus open new door for facile detection of trace amount of molecules in important areas of medical diagnostics and food control. In order to exploit this method in these fields, a technique that enables cost-effective fabrication of plasmonic nanostructures over large areas needs to be developed. This thesis concerns laser interference lithography for the preparation of two dimensional arrays of metallic nanoparticles that holds potential for strong amplification of fluorescence signal. The investigation of lift-off fabrication of the plasmonic nanoparticle arrays by using a photoresist mask with arrays of holes or arrays of disks is pursued. Different developers, etching parameters, exposition dose, concentration and type of the developer, dilution of the resist, and soft baking temperature were systematically optimized. A bi-layer system consisting of a spacer layer enabling undercut and a top photoresist film was tested in order to facilitate the lift-off. This approach avoids problems such as thermal cross-linking of the resist after dry etching and prevents the entire coating of the system after gold evaporation. The obtained patterned structures were characterized using atomic force microscopy and scanning electron microscopy.

Contents

List of abbreviations

LIL	Laser Interference Lithography
LSPs	Localized Surface Plasmons
cLSPs	Collective Localized Surface Plasmons
AFM	Atomic Force Microscope
SEM	Scanning Electron Microscope
BRE	Biological Recognition Element
FRET	Förster Resonance Energy Transfer
SPR	Surface Plasmon Resonance
SPPs	Surface Plasmon Polaritons
PEF	Plasmon Enhanced Fluorescence
MEF	Metal Enhanced Fluorescence
EF	Enhancement Factor
DNQ	Diazonaphthoquinone
ICA	Indene Carboxylic Acid
TM	Tranverse Magnetic
TE	Transverse Electric
PMGI	Polydimethylglutarimide
TMAH	Tetramethylammonium Hydroxide
NaOH	Sodium Hydroxide

1. Introduction

Fluorescence has arguably become the dominant technology for the analysis of biomolecules and is extensively used in areas such as medical diagnostics and biotechnology. It offers the advantage of high sensitivity and in specific cases even individual molecules can be analyzed. However, in practical assays for the detection of chemical and biological species such as biomarkers in bodily fluids, detection limits needs to be advanced in order to improve non-invasive medical diagnostics that rely on the analysis of trace amounts of these compounds. Near field optics has been largely investigated to advance fluorescence-based techniques and improve their sensitivity. Among these, plasmonics was showed to allow for extreme confinement of electromagnetic field intensity through coupling light to surface plasmons at metallic nanoparticles and nanostructured metallic thin films. This confinement is accompanied with strong enhancement of the field strength that can massively amplify the fluorescence signal emitted from fluorophores that serve as labels in fluorescence bioassays [1]–[4]. Over the last years, we witnessed efforts been made towards developing of sensors that exploit this so-called plasmonic enhancement effect to advance detection limits of fluorescence bioassays for the analysis of analytes [5], [6].

Fluorescent amplification is closely related to the strength of the surface plasmon field generated in the proximity of metallic surfaces. Therefore, several structures has been designed and investigated for providing field intensity enhancement $|E|^2/|E_0|^2$ such as nanoholes or nanodisk arrays [7], flat [8] and corrugated metallic films [9], and metallic nanoparticles [10]. Among these structures, Au nanoparticles dimers stand out with field intensity enhancement of two orders of magnitude [11], [12]. The highest plasmonic fluorescent amplification reported experimentally provide an enhancement factor EF=1340 for a bowtie nanoantenna structure (triangle nanoparticles with 30 nm gap) with a low intrinsic quantum yield dye (η^0=0.025) [13]. Previous simulations carried out in our group show that diffractive array of metallic nanoparticles supporting collective localized surface plasmons (cLSPs), exhibit particular strong field intensity enhancement as well. This great increase of field intensity of about 2 orders of magnitude, compared with individual metallic particles, is due to the reduced radiative damping of LSPs modes in a symmetric refractive index environment. Several simulations were carried out placing an assumed fluorophore in the vicinity of such field, leading to a theoretical enhancement factor (EF) of 3 orders of magnitude in the fluorescence light emitted by the fluorophore. This result arises from the raise in quantum yield, increment in excitation rate, and direction of the far field angular distribution of the emitted light through surface plasmons [14].

Research in plasmonics that takes advantage of metallic nanostructures was mostly carried out by using precise methods such as electron beam lithography and focused ion beam milling [15]–[17]. However, these methods are not suitable for exploiting plasmonics in practical applications as they are time consuming and does not allow for structuring of large areas. Nanoimprint lithography and colloidal lithography were developed in order to overcome this drawback. Nanoimprint lithography allows producing large amount of copies of structures that are prepared by, e.g., electron beam lithography by a transfer of the motif to a thermo-polymer or UV cross-linkable polymer films. By techniques such as roll-to-roll

[18], [19], mass production can be facilitated, but the initial investment to produce the master are high. Colloidal lithography is a bottom down approach that based on self-assembly and it holds potential for extremely cheap preparation of metallic nanostructures that can be adopted both in the laboratory or up-scaled [20], [21]. However, this method inevitably suffers from formation of defects and separation of the structure into irregular domains. This thesis focuses at using laser interference lithography (LIL) for preparation of metallic nanostructures with tailored plasmonic properties. It is an established technology for fabricating of periodic nanostructures over large surface area with minimum defects. Contrary to nanoimprint lithography, it does not require using of expensive masters and offers the advantage of high degree of flexibility suitable for rapid prototyping [22]. LIL has been used for preparation of Au gratings [23], plasmonic gold nano-rings arrays [24], metallic disks [25], or gold nanodisk arrays [26]. LIL was adopted for preparation of metallic nanoparticle arrays by using lift-off [27] and in this work, a glanced angle deposition of a metallic film on a photoresist mask with arrays of nanoholes was used, allowing for efficient lift-off.

1.1 Biosensor technologies

Established analytical methods, such as gas/liquid chromatography and mass spectrometry, allow for detection and quantification of analytes of very low concentration. Nevertheless, these techniques are complex, time consuming and require trained personal for operating them. Contrarily, biosensor detection systems are pursued to complement these techniques and provide fast, portable and cost-effective analysis. Some of these systems are capable of in situ and real time detection with very high specificity [28]. Therefore, biosensing technologies are attractive for many applications in healthcare, food industry, environmental monitoring and similar sectors, and research is being continuously conducted to develop novel biosensors and biomarkers [29].

A biosensor is an analytical sensing device, which employs a biorecognition element (BRE) in close connection with a physical transducer for the analysis of chemical and biological species. The interaction between BRE and analyzed species is translated into a measurable signal proportional to the concentration of the chemical entity investigated [30]. The BRE is one of the key parts in a biosensor device and is chosen regarding its affinity and specificity. There is a wide range of bioassays using antibodies, cells, enzymes, aptamers or nucleic acids as bioreceptors elements [31]. Regarding the transduction system, biosensors can be classified into several groups: optical, electrochemical, thermometric, magnetic and piezoelectric. The detection system in optical biosensors is based on the change in an optical property, upon interaction of the BRE with the target, for instance, changes in luminescence, absorbance, refractive index, light scattering or polarization [32]. Fluorescence based-detection is extensively used due to its high sensitivity and selectivity. A fluorescence assay relies on the detection of electromagnetic radiation emitted by a fluorophore returning to its ground state, which previously has been excited to a higher singlet state by absorbing photons [33].

Most of the optical biosensors use the evanescent field for probing, creating different sorts of biosensors: surface plasmons resonance (SPR), interferometers, resonant mirrors, or planar array fluorescence sensors [34]. These sensors detect surface-binding events in real time. Evanescent wave probing can be obtained through several coupling schemes as total internal reflection using prism coupling or Kretchmann's configuration, wave guide optical fibers or gratings. Among the different sorts of optical biosensors, SPR based biosensors exhibit some advantages such as fast response, label-free technique and high refractive index sensitivity. Labels can be added when a further amplification of the response is needed.

1.2 Surface plasmon resonance (SPR)

Surface plasmon resonance originates from collective electron oscillations at the interface between metal and dielectric, which exhibit real part of permittivities of opposite sign. Surface plasmons polaritons (SPPs) are traveling waves at the continuous metal surface. Localized surface plasmons are surface plasmons supported by metallic nanostructures. Both types of surface plasmons are illustrated in Figure 1.

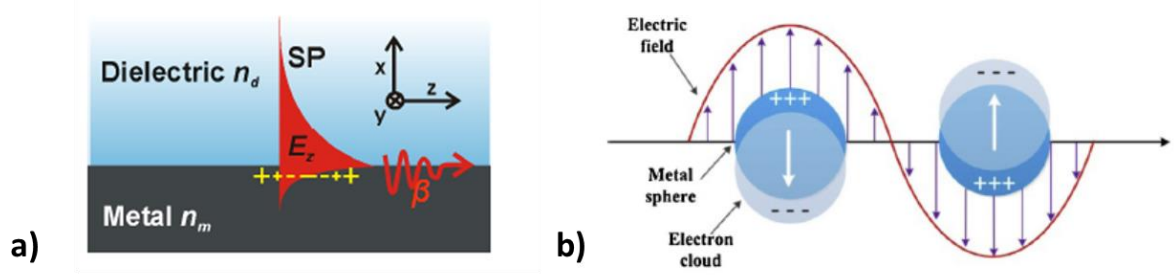

Figure 1. Schematic of metallic structures supporting: a) SPPs and b) LSPs [35].

SPPs can be excited with flat or corrugated continuous surfaces. Regarding LSPs, the shape and size of the metallic structure is one of the most influential factors to control the spectral properties. Consequently, many approaches have been conducted to synthetize different shapes such as nanorods, triangles, octahedrons, spheres or prisms, which achieve tailored LSPR excitations from infrared to visible regions [36], [37]. The coupling of these surface plasmons with the light enables the confinement and enhancement of the electromagnetic field intensity [38]. Excitation of LSPs can be achieved when the light directly hits the metallic structures and coupling scheme is not required as in SPPs. In consequence, more flexible and lower cost sensor devices can be fabricated [35].

In a SPR setup the incident light is coupled to surface plasmons and the measured reflected light intensity shows a sharp attenuation in the measured reflectivity (SPR minimum). The wavelength or incident angle where the resonance occurs is highly sensitive to the local refractive index variations in the vicinity of the metallic structures. Typically, when the refractive index increases, the resonance shifts to higher incident angle or wavelength. The binding of BRE changes the local refractive index, shifting the SPR minimum and enabling to monitor the surface binding in real time [39]. Current limit of detection for direct SPR based biosensors is about 1 pg/mm^2, which often insufficient for detecting low

concentrations of analytes [40]. Research at the nanoscale for SPR biosensors is focused on the design of nanostructures and nanomaterials for signal enhancement [41].

The interaction of a fluorophore with the enhanced field intensity, which is created through coupling of the light with surface plasmons, can alter favorably its properties. This alteration in the emitter performance leads to an increased fluorescence signal. This effect is known as metal enhanced fluorescence (MEF) or surface plasmon enhanced fluorescence (PEF) and paves way for new detection schemes. For instance, a surface plasmon resonance system can be employed for excitation of a dye located in the proximity of metallic nanostructures and the emitted signal can be collected with a detector. Limits of detection in the femtomolar concentration range have been achieved with PEF method [42].

1.3 Surface plasmon-enhanced fluorescence (PEF)

The interaction of fluorophores with confined electromagnetic fields of surface plasmons has been investigated by numerous studies with organic dyes or quantum dots [43], [44]. This intense field of surface plasmons, together with the increase of local optical density of states, enables to raise quantum yield, increase excitation rate, and control the far field angular distribution of fluorescence light emitted by the fluorophores. When a fluorophore emitter is placed in proximity to metallic nanostructures, decay rates are modified and the lifetime of the chromophore group can be highly reduced, changing the quantum efficiency [45]. This effect is especially important for fluorescent emitters with a low intrinsic quantum yield, which hold intrinsically better potential for enhancement by the metallic structure. The excitation rate at absorption wavelength (λ_{ab}) of the emmiter can be amplified through this plasmonic-mediated excitation. The distance between the metal and the emitter affects strongly the interaction, since at distances shorter than 15 nm strong quenching of the radiative states is observed due to Förster resonance energy transfer. At longer distances, substantial fraction of the radiation intensity can be emitted through surface plasmons and be resonantly out-coupled to a certain angle, which allows concentrating the emitted light towards the detector [46]. Overall, this coupling permit amplification of the fluorescence signal associated with molecular binding events by several orders of magnitude [47]. These three effects for the enhancement factor (EF) of collected fluorescence are summarized in Eq. 1.

$$EF = \frac{\gamma_e}{\gamma_e^0} \times \frac{\eta}{\eta^0} \times f_d \quad (Eq.1)$$

Where $\frac{\gamma_e}{\gamma_e^0}$ is the enhanced excitation rate at fluorophore λ_{ab}, $\frac{\eta}{\eta^0}$ is the increasing quantum efficiency by decreasing lifetime of fluorophore excited state, and f_d is the directional emission at emision wavelength (λ_{em}) of the emitter, which enables efficient detection of fluorescence light intensity. The EF of fluorescence is calculated with respect to that measured without the plasmonic structures (e.g., free fluorophore located in an aqueous environment).

The plasmon enhanced fluorescence (PEF) effect depends on a variety of parameters such as metal composition, particle size and separation, fluorophore type, and fluorophore-

particle separation [48], [49]. These structures have different ability to confine and enhance the EM field, being the ones who generate the maximum field intensity enhancement the most promising for PEF amplification [50].

A plasmonic system with a periodic array of metallic nanoparticles can support collective (lattice) localized surface plasmons. Such structure is able to trap light at surface more efficiently and exhibit decreased radiative damping, especially in a refractive index symmetrical geometry (e.g, same refractive index below and above the particle array). This light-trapping enhancement and radiative damping decrease, is produced when metallic particles exhibit a periodicity that is near to the wavelength employed for the phase-matching of LSPs. Under this condition, the light diffracted by some particles can be collected from the neighboring particles leading to sharp resonances and electric field enhancement [51], [52]. This diffractive coupling results from phase matching of LSPs at wavelengths that correspond with the LSPR band of individual nanoparticles [53]. Diffractive arrays of metallic nanoparticles provide highly directional fluorescence emission, allowing the control and direction of the emission towards a detector. Finite difference time-domain (FDTD) simulations of a cLSP array made of gold disk nanoparticles, with similar refractive index below and above the cylindrical gold particles, showed a field intensity increase of $|E|^2/|E_0|^2 = 2\times10^2$ at λ=630–670 nm wavelength (see Figure 2) [14].

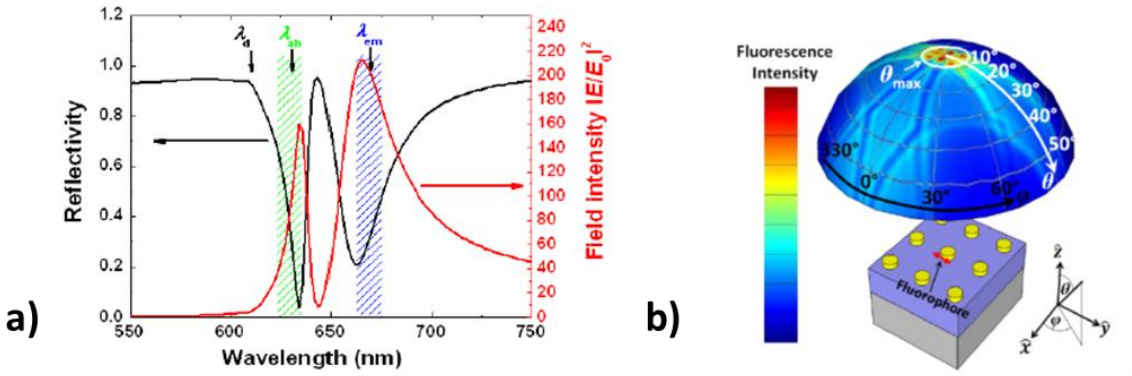

Figure 2. a) Wavelength spectrum illustrating electric field intensity enhancement and reflectivity b) Far field emission of a fluorophore placed in a structure supporting cLPs [14].

The structure was tailored to support two resonances in the vicinity of the λ_{ab} and λ_{em} wavelengths of a simulated fluorophore, as shown in the reflectivity spectrum in Figure 2 a). For instance, AlexaFluor647 (λab=650 nm, λem=665 nm) or Cy5 dye (λab=640 nm, λem=670 nm). The electric field intensity enhancement is estimated at a point established at 20 nm from the cylindrical disk. The coupled emission with cLSP confines far field emission in a precise angular cone as shown in Figure 2 b). This directivity at polar angles below θ=8.5 deg. enables a high collection efficiency of CE=5.2 % for a numerical aperture of NA=0.2.

2. Goals

The aim of this thesis is to establish laser interference lithography for the fabrication of metallic nanostructures that holds potential for strong amplification of fluorescence signal in bioassays. In particular, this method is to be adopted for preparation of Au disk arrays over area > 1 cm^2. This work supports research in exploiting of structures supporting collective localized surface plasmons that were identified as promising means for extremely high fluorescence signal amplification in the previous studies [14]. An example of the structure is given in Figure 3 and it is composed of rectangular arrays of cylindrical Au particles with a period of Λ=460 nm, diameter of D=110 nm and height h=50 nm as determined by simulations and verified by experiments [54]. The particles are placed on top of a low refractive index layer, assumed to be Cytop (n=1.34) or Teflon AF (n=1.32), with a thickness of d=120 nm. This layer is located above a BK7 glass substrate with a silver coating.

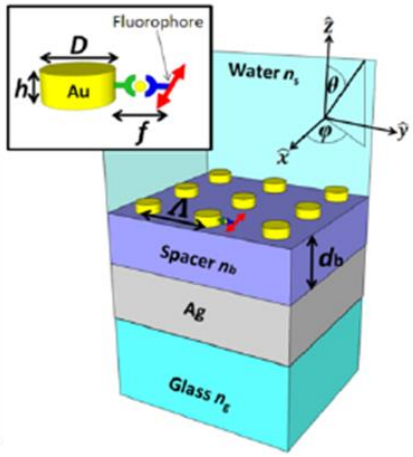

Figure 3. Schematic of the aimed nanostructure supporting cLSPs [14].

The preparation of Au nanoparticle arrays on a dielectric substrate will be pursued in several steps and systematic optimization of each of them:

1) LIL-based preparation of a photoresist mask with A) arrays of nanoholes on a dielectric substrate or B) arrays of photoresit disks on a thin metallic layer.
2) For the arrays of nanoholes A), a thin Au layer is subsequently deposited by vacuum thermal evaporation and the nanoparticles formed in the mask protrusions are prepared by lifting off the photoresist mask.
3) For the arrays of photoresist cylinders B), the mask structure is transferred to the underneath Au film by using dry etching.
4) A bi-layer system with an undercut layer below the photoresist mask is to be developed in order to improve the lift off and potentially enable to fabricate smaller structures, which are limited by the steepness of the photoresist nanohole or nanodisk walls.

3. Experimental methods and materials

3.1 Laser interference lithography (LIL)

Photolithography is a well-established technique in semiconductor industry for fabrication of micro and nanostructures. The principle of lithography relies on the transfer of a geometric pattern carried by a mask into a photosensitive material (photoresist). LIL is a technique based on two or more highly-coherent laser beams, which form an interference pattern when the light beams superimpose. Light from a source is split and recombined to create a standing wave pattern and this interference pattern can be recorded on a photosensitive substrate [55]. Theoretically, the smallest feature size that can be reached using interference lithography depends on the employed light source, being half of the wavelength of the laser ($\lambda/2$). Mainly two setups are used for LIL: a) The Lloyd's mirror interferometer and b) dual beam interferometer. In the dual beam interferometer setup, the incidence angles of the two beams are adjusted separately. Consequently, in order to change the period of the grating, the setup has to be rebuilt and re-aligned. In addition, the difference in the optical path of the two beams make the system more sensitive to airflow and a phase correction system is needed to compensate any change in phase due to this airflow. The advantage is that larger areas can be exposed [56]. The Lloyd´s mirror Interferometer (see Figure 4) is composed of a mirror placed perpendicular to the sample holder. Both are mounted on a rotating stage, which enables an accurate and easy change of the period by changing the angle. One part of the light beam is reflected on the mirror and interferes with the portion of the beam that directly illuminates the sample. This setup provides mechanical rigidity reducing vibrations and creating well defined patterns even for longer exposure time [57].

For two interfering planar waves the period of the interference intensity pattern is a function of the angle (θ) and wavelength (λ) as Eq. 2:

$$\Lambda = \frac{\lambda}{2\sin\theta} \qquad (Eq.2)$$

Two interfering laser beams from the same source create an intensity pattern consisting of dark and bright fringes. The intensity and phase relation of this pattern can be described as Eq. 3 [56].

$$I_s = I_1 + I_2 + 2\sqrt{I_1 I_2} * \cos\varphi \quad (Eq.3)$$

Where φ, ($\varphi = \frac{2\pi}{\Lambda}x$), is the phase difference due to the path difference between the two beams. Notice that the intensity is changing with the cosine of the phase only in x-direction, which is the plane of incidence. I_s is the resulting intensity when the beams interfere. I_1 and I_2 are the intensity of each beam separately.

The fabrication of nanostructures is limited to periodic structures such as dots, holes, gratings, and variations on them. Two-dimensional structures can be achieved by exposing the resist multiple times, rotating the substrate after each exposure.

In this work, Lloyd's Mirror Interferometer was employed for the lithographic exposures as depicted in Figure 4. A 4 mW HeCd laser (model IK 3031 R-C from Kimmon) was used to generate a highly coherent light beam at λ=325 nm. A spatial filter (40x microscope lens and pinhole with diameter d=10µm) expands the beam making its intensity profile homogeneous. An additional lens (f=100 cm) located 1m away of the pinhole is used to collimate the beam. The sample holder with a rectangular dielectric mirror (RM-50.0-30.00-12.7-UV, CVI Melles Griot) was placed away from the spatial filter, and the distance was chosen in a way that results in a larger exposed area on sample. The angle was easily adjusted with the rotating stage to obtain the desired period by using Bragg's condition (Eq.2). The power of the laser at the sample holder was around 32 µW/cm^2. The exposition dose is calculated multiplying the power with the exposition time (1 mJ/cm^2 = 1 sec x 1 mW/cm^2). The complete setup was built on an actively damped optical table to prevent vibrations.

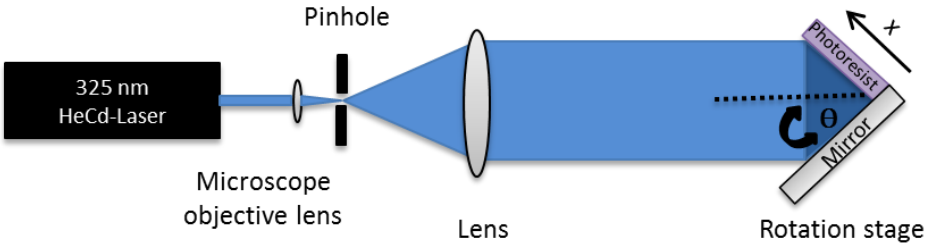

Figure 4. Schematic illustration of the Lloyd's-Mirror Interferometer set up.

3.2 Photoresist

The selection of the photoresist needs to take into account the characteristic of the fabrication process. Negative photoresists crosslink after exposure, and subsequent baking step, while the non-exposed regions are dissolved by the developer. These resists are thermally stable and elevated temperatures will not deteriorate the resist profile. Nevertheless, the wet-chemically etching becomes more difficult with the increase of crosslinking of the resist, making it even impossible to remove. On the other hand, positive photoresists are mainly made of diazonaphthoquinone (DNQ) derivatives mixed with a phenolic resin (Novolac resin). Phenolic resins are hydrophilic and can be dissolved by aqueous alkaline solutions due to the OH groups. The DNQ acts as a dissolution inhibitor when is mixed with phenolic resins by making the mixture hydrophobic. During the exposition DQ is converted into indene carboxylic acid (ICA) which is hydrophilic and therefore the exposed regions turn out soluble for the alkaline developer (alkaline solution) [58]. The DNQ primary photoreaction is depicted in Figure 5. The inhibition of the Novolac resin by DNQ derivatives is essentially a physical phenomenon caused by an electric stress imposed on the phenol groups of the resin by the inhibitor [59].

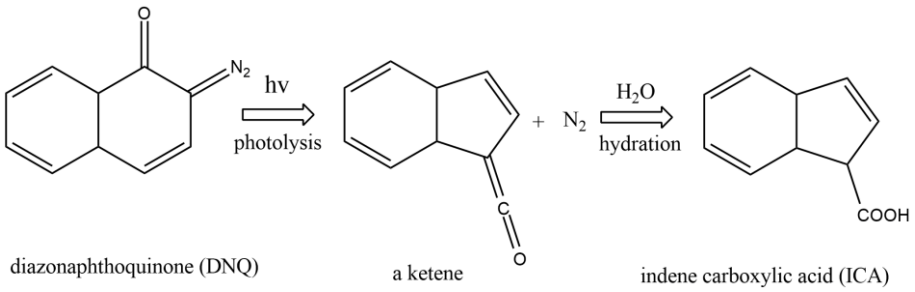

Figure 5. DNQ primary photoreaction.

Contrast is limited using negative photoresist due to the crosslinking reaction occurring after exposure. Consequently, in this work a Novolac resin based positive photoresist (S1805 G2 photoresist) is employed due to several advantages such as high contrast, good step coverage, and high aspect ratios [60]. Another important aspect in the lithographic procedure is the soft-baking of the resist prior the exposition. This step removes the solvent, making the coating sensitive for the lithography. Both, over and under-softbaking will hinder the resist performance. After exposure, the exposed regions have to be developed, for positive resists, solubility increase with exposition dose. Dissolution rate versus exposure, developing time, pre-baking temperature or concentration of the developer are the typical parameters that have to be optimized to obtain the desired nanostructures.

3.3 Materials

S1805 G2 positive photoresist was purchased from Microresist Technology (Germany). The solvent for the resist, propylene glycol monomethyl ether acetate, was obtained from Sigma-Aldrich (Schnelldorf, Germany). LOR1A polymer employed as a lift-off layer, composed of polydimethylglutarimide, was ordered from Microchem (MA, USA). PG remover solution to achieve the lift-off was purchased from Microchem (MA, USA) as well. AZ-303 developer based on concentrated sodium hydroxide (NaOH) was obtained from AZ electronics materials (Germany). MF-26A developer based on tetramethylammonium hydroxide (TMAH) 0.26N was obtained from Microresist technology (Germany). Microscope glass slides with 2.0 x 2.0 cm^2 dimension for LIL were purchased from Thermoscientific (Germany). Hellmanex III solution for cleaning the surface of the glass slides was obtained from Sigma-Aldrich (Schnelldorf, Germany).

3.4 Experimental procedure

3.4.1 Glass substrate preparation

Samples were produced with 2.0 x 2.0 cm^2 microscope slides immersed first in 2 % Hellmanex III solution followed by an ultrasonic bath for 30 min. Then, the glass substrates were rinsed with distilled water and an additional ultrasonic bath for 30 min. was made. Afterwards, samples were rinsed with water and placed again in the ultrasonic bath for 30 min. with ethanol. Prior to the spin coating process the substrates were removed from the ethanol solution and dried with an air gun.

3.4.2 Cross-gratings preparation

Glass substrates were spin-coated at 4500 rpm for 45s with Microposit S1805 G2 positive photoresist diluted (1:2) with propylene glycol monomethyl ether acetate. Afterwards, samples were softbaked for 2 minutes at 98°C on a hot plate. A black tape was attached on the back side of the glass substrates. This step suppresses the reflection of the laser beam back into the resist. The interference pattern was recorded on the S1805 resist using the Lloyd's mirror interferometer setup described in 3.1. The samples were first exposed and then rotated by 90° and exposed for a certain time to obtain periodic two-dimensional structures (holes/particles) with same periodicity. The angle was adjusted to 20° in order to set the period to Λ=475 nm. Then, exposed substrates were developed in AZ-303 developer solution with deionized water (1:15) or with MF-26A developer at various concentrations (1:0.25-1:0.35). Different developing times were employed to achieve the photoresist mask geometry. After each development, substrates were rinsed with copious amounts of deionized water and dried under air gun. All the steps were performed under yellow light.

Regarding the bi-layer system including a lift-off layer, substrates were spin-coated with LOR1A lift-off polymer at 4000 rpm for 60s. Prior to the spin-coating, glass substrates were left on a hot plate for 5 min at 150-185°C. Afterwards, substrates were softbaked for 2-5 minutes at 150-185°C on a hot plate. The second layer was spin-coated at 4500 rpm for 45s with Microposit S1805 G2 positive photoresist diluted (1:2) with propylene glycol monomethyl ether acetate. Substrates were softbaked for 2 minutes at 98°C on a hot plate. Same procedure and conditions were used for the exposition and development as mentioned above for the substrates coated with the photoresist. All the steps were performed under yellow light.

3.4.3 Dry etching

Ar ion beam milling (Roth & Rau IonSys 500) was employed as a dry etching or physical etching method. The conditions employed are shown in Table 1.

Table 1. Argon milling parameters

Angle(º)	50
Rotation(rpm)	3
Plasma(W)	42
Beam(V)	500
Accelerator(V)	500
Pulse width(%)	75
Process time[etch+pause] (min)	8+16

The other method utilized for dry etching procedures was an oxygen plasma etching system (Femto plasma cleaner, Diener electronic). The power was adjusted to 40% and the process time was varied between 3-5 min.

3.4.4 Metallic film deposition and lift-off solution

Gold deposition was performed by thermal evaporation (HHV AUTO 306 from HHV LTD) in vacuum (1 x10^{-6} mbar). 2 nm Cr and 50 nm Au layers were subsequently deposited into the patterned substrates. Cr was used as a promoting adhesion layer. Finally, the lift-off was carried out immersing the sample in a stirred PG remover solution. The time for the lift-off can vary from minutes to hours, which can be speed up by using an ultrasonic bath (Elmasoni S10).

3.4.5 Observation of nanostructures

The fabricated structures were characterized using Atomic Force Microscope (Picoplus, Molecular Imaging, Agilent technologies) and Scanning Electron Microscope (ZEISS Supra 40 VP). The AFM was operated in the AAC tapping mode using the small scanner. The cantilever utilized was PPP-NCHR (Nanosensors). The data analysis of the SEM and AFM images was carried out with Gwyddion software (open-source software for scanning probe microscopy data processing).

3.4.6 Etching rate estimations using Surface Plasmon Resonance (SPR)

Towards a better understanding of the development process, the etching rates of the S1805 positive photoresist and the LOR1A sacrificial layer were estimated with a SPR system for two different developers. AZ-303 developer and MF-26A developer were analyzed. A transverse electric (TE) and a transverse magnetic (TM) polarized beam of a He-Ne laser (25-STP-912-210 from CVI, power 2mw) at a λ=632.8 nm was coupled to a high refractive index BK7 glass prism (n_p=1.845). A sensor chip optically matched using immersion oil was placed on the base of the prism. The sensor chip consisted of a glass slide evaporated with 2 nm Cr and 50 nm Au layers. S1805 and LOR1A layers were spin-coated separately above the gold layer. The coated chips with the resist and the sacrificial layer were measured before and after the immersion inside the developer solution for a certain amount of seconds. The thicknesses of the layers were obtained by fitting the measured reflectivity curves with the transfer matrix model implemented in the Winspall software (developed at the Max Planck for Polymer Research in Mainz, Germany). The etching rate was calculated subtracting the thickness of the remaining layer (after development) to the initial thickness of the coating. Followed, this value was divided by the seconds that the substrate was immersed in the developer solution. Regarding the exposition of the photoresist, samples were placed in the same lithographic set up as mentioned in 3.1 except for the mirror, which was carefully removed. This enables to expose uniformly, using the same conditions used for the fabrication of the structures, the entire surface of the resist without having an interference pattern with bright and dark regions. Samples were kept under exposition 4 times longer in comparison of the resist samples in the 3.4.2 section. This pretends to mimic the bright intensity regions with 4 fold higher intensity than the dark regions with destructive interference pattern (Eq.3). These higher dose areas with twice maximum intensity exposure (constructive interferences) lead to holes after development, being the region of interest for our undercut rate studies.

4. Results and discussions

The investigated layer structure and lift-off process is illustrated in Figure 6. It consists of a substrate coated by LOR1A sacrificial layer with a thickness of d_L=120 nm measured by SPR and AFM. On the top of the LOR1A layer, a photoresist S1805 film was prepared with a thickness of d_p=100 nm. After recording the UV interference light pattern, the bi-layer structure was etched by a developer. The work described below concerns design of the layer parameters and exposition / etching conditions that allows for reliable preparation of Au nanoparticle arrays by the lift-off process. In general, alkaline developers dissolve LOR1A isotropically, which enables to achieve an undercut in this sacrificial layer and allow for easier lift-off. As described further, the etching characteristics were investigated in order to tune and etch faster to the LOR1A sacrificial layer than to the photoresist S1805. The fabrication process for the two approaches named as A) and B) is shown in Figure 6. For the approach marked as A), Au layer with a thickness of h=50 nm is evaporated on the polymer mask prepared on a glass substrate, prior this step coating, exposition and development of the layers has been carried out. The thickness of the LOR1A layer was chosen to be above the height the Au nanoparticles (h=50 nm). For the approach B), the mask was prepared on a glass substrate carrying a 50 nm thick Au film, followed by the coating, exposition and development of the layers. Afterwards a dry etching method is employed to etch the gold and the subsequent lift-off originates the metallic structures. The thickness of the LOR1A can be smaller and the photoresist can be tuned.

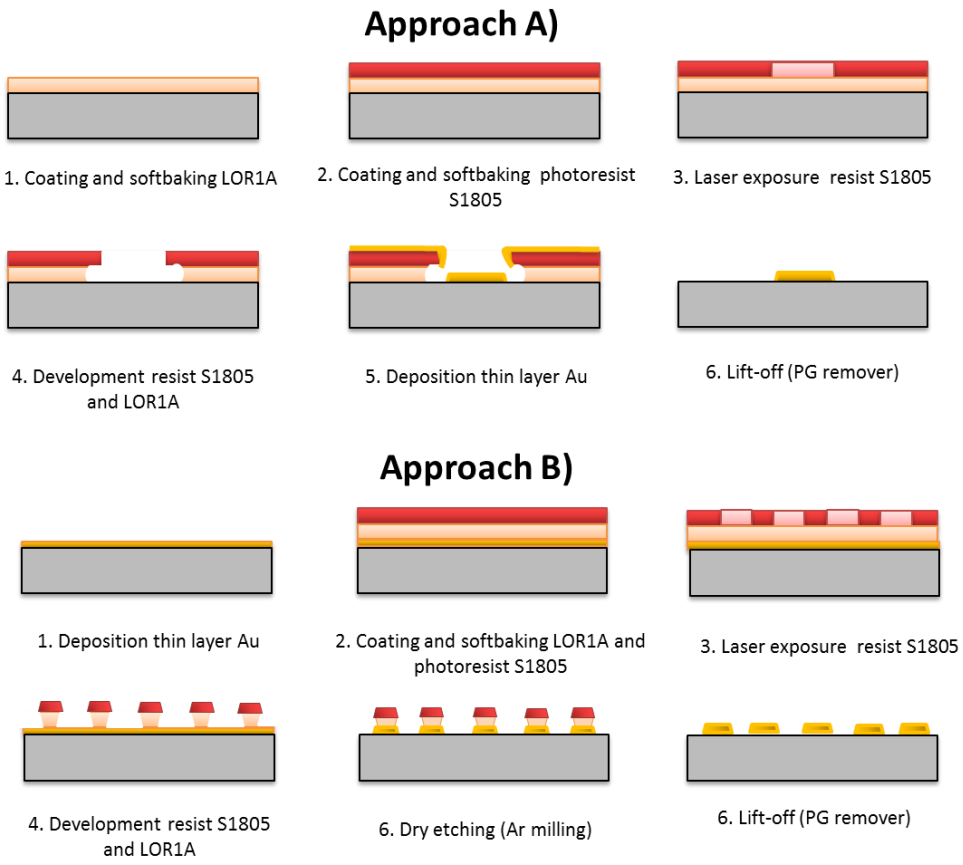

Figure 6. Fabrication procedure of metallic nanostructures with a lift-off layer: Approach A) and B).

4.1 Etching rates of S1805 resist and LOR1A sacrificial layer

To control etching rate to the S1805 layer $r_p=\Delta d_p/\Delta t$ and to LOR1A layer $r_L=\Delta d_L/\Delta t$, the exposition dose, soft baking temperature, and concentration and composition of the developer was tuned as described below. It should be noted that the etching rates were measured for flat polymer films and that only the photoresist S1805 was sensitive to irradiation by UV light while the LOR1A was not affected by UV.

4.1.1 AZ-303 developer

The etching rates measured with SPR for the AZ-303 developer are compared in Figure 7 for varied soft baking temperature and baking time. From the bar graphs one can see that the etching rate to LOR1A r_L is 2-3 times lower than the etching rate of the photoresist S1805 r_p that was exposed to the UV light dose of 460 mJ/cm^2 (115 mJ/cm^2 multiplied by four, see 3.4.6). When comparing the etching rates for the photoresist layer not exposed to UV light, the LOR1A layer can be tuned to exhibit about 4.5 higher etching rate. Let us note that sufficiently high etching rate ratio r_L/r_p is needed for a well-defined undercut when a single wet etching step is used. Notice that the temperature used for the baking of the LORA layer was 150 °C, which is the lower temperature recommended for PMGI polymers. Consequently, when higher temperatures are applied for baking the LOR1A, the etching rate ratio would be lower. In summary, the etching rate ratio can be tuned with the softbaking temperature and time for the used materials and AZ-303 developed diluted by water 1:15. However, notice that the etching rate of the LOR1A should be higher than the etching rate of the exposed resist to enable a well-defined undercut formation.

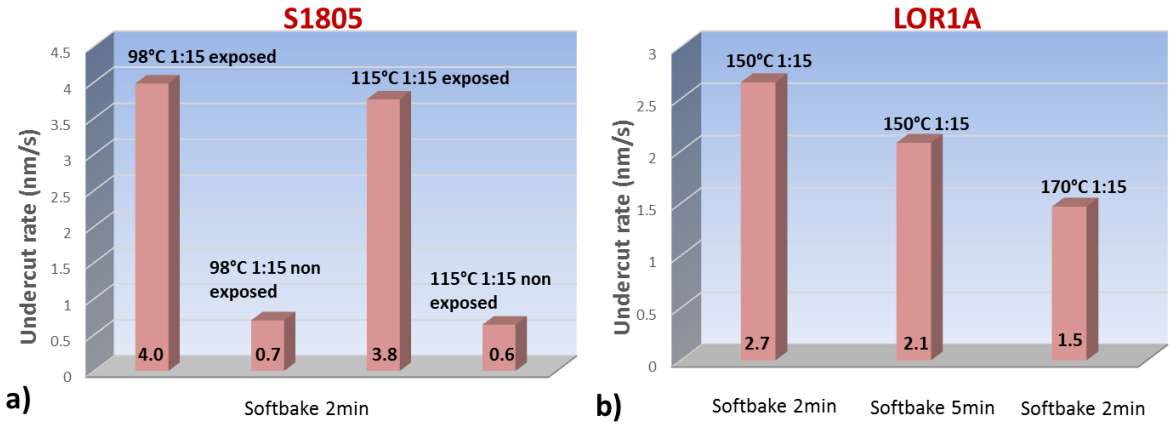

Figure 7. Etching rates determined for a) S1805 resist and b) LOR1A polymer with 1:15 ratio AZ-303 developer solution at different temperatures.

4.1.2 MF-26A developer

The measured etching rates for an alternative developer MF-26A are summarized in Figure 8. The etching rate of the LOR1A can be effectively controlled with the baking step, by changing the temperature and the time of the sample at the hotplate, or by varying the

dilution ratio of the developer. The TMAH based developer etches faster the sacrificial layer than the photoresist layer fulfilling the criteria for creating a proper undercut. The LORA baking recommended temperature is between 150-200 °C, and the undercut rate decreases by increasing the temperature. Same trend is observed for the dilution of the developer with deionized water, lowering the etching rate upon dilution. The undercut rate is a critical factor in the nanofabrication process since at higher etching rates the lift-off resist dissolve too fast, which makes the control of the process difficult and causes detachment of the layers from the substrate. When the pure developer is employed (1:0) the etching rates for the LOR1A r_L are too high for our bi-layer system and a dilution of the developer is required. For 150-170 °C temperature range, 1:0.5-1:0.75 dilution ratio provides an interval with adequate characteristics for an optimum lift-off control. For 185°C a smaller dilution can be used (1:0.2-1:0.25) to obtain suitable etching rate values.

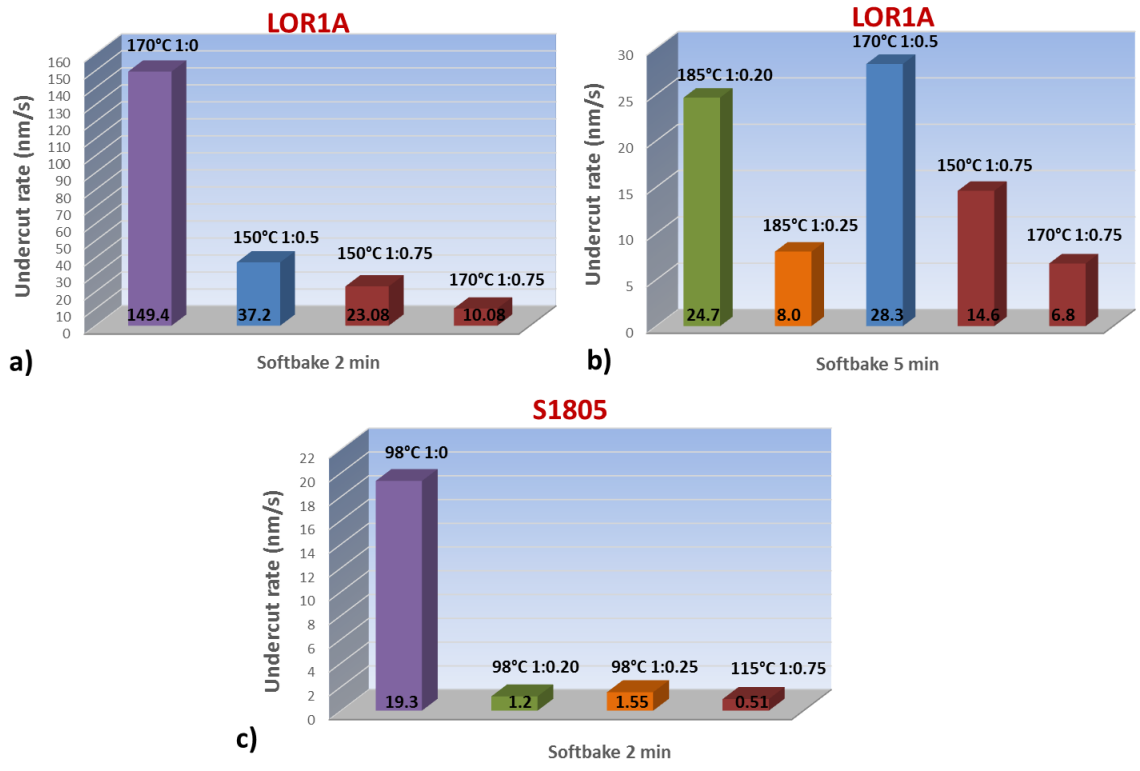

Figure 8. Etching rates determined at different temperatures and dilution ratios of the developer for a) LOR1A with 2min softbake b) LOR1A 5min softbake c) exposed S1805 with 2 min softbake employing MF-26A developer.

On the other hand, the development rates for the S1805 resist upon dilution of the developer (for 460 mJ/cm^2) are quite low in comparison with those of the LORA layer. This fact impedes a well-defined aspect ratio of the resist templates because the development time increases, which increases the dark erosion and hinder obtaining a good contrast profile. The undercut rate of the resist can be increased with the exposition time while the LORA undercut rate is not affected by UV light. Therefore, a protocol providing a good contrast with suitable and controllable undercut rate has to be established to obtain templates with our bi-layer system. In summary, the using of other developed MF-26A allows to achieve much higher etching rate ratio r_L/r_p=5-30. It should be noted that this

values takes into account only the photoresist layer that was exposed to the UV light with the dose of 461 /cm^2. Therefore, for the unexposed photoresist this ratio would be even much higher.

4.2 Photoresists mask templates using AZ-303 developer

A protocol was developed to fabricate periodic 2D masks into S1805 photoresist by using the AZ-303 developer. As described below, masks with square symmetry were prepared by using LIL with two subsequent exposures each with the dose 57.5 mJ/cm^2. By varying the developing time, the mask can be tuned to exhibit either narrow nanoholes or small nanoparticle arrays.

These structures comes as the result of the interference pattern recorded to the photoresist, which leads to spatially varying etching rate r_p at the areas exposed to strong and weak UV light intensity. This can be seen in Figure 9 where the three different intensity regions lead to formation of a nanohole array. “C” squares are the constructive interference regions, which are double exposed with maximum intensity. “D” squares are the destructive interference areas, exposed twice with minimum intensity and “S” squares are the middle areas which have been exposed once to the maximum and once to the minimum.

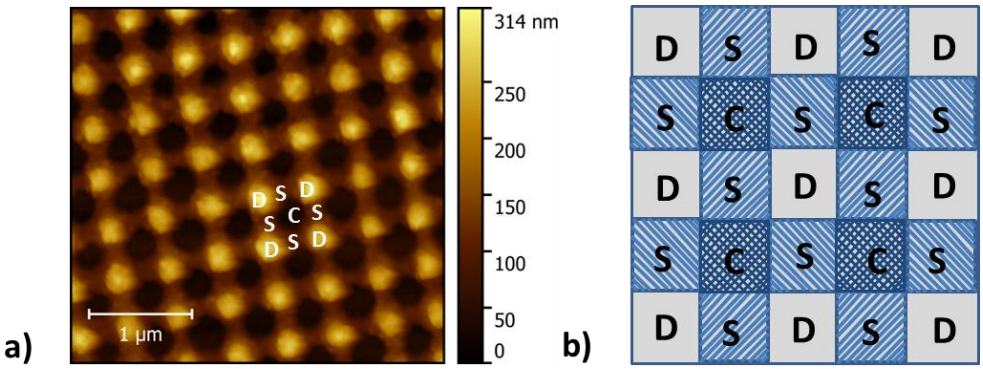

Figure 9. AFM images of the nanoholes arrays: a) 2D view for 30s development, exposure time 4x4min, 1:1 resist dilution ratio, 1:15 developer dilution ratio b) schematic of the different intensity regions.

The low beam intensity of the laser used for our lithography set up is not suitable for thick resists and a thin resist layer is needed to reach the glass surface while maintaining well-defined aspect ratio of the template. For this reason, a dilution of the photoresist with the solvent was made. In Figure 10 one can see the symmetric template arrays made of photoresist obtained by varying the development time for 1:2 dilution ratio of the resist. Notice that after 30-35 s. the nanoholes mask is formed and a further increase in developing time lead to the nanoparticles mask around 50-55 s. The thickness of the photoresist coating was approximately 100 nm for 1:2 dilution ratio, calculated using SPR and AFM systems for a spin rate of 4500 rpm. The thickness can be modulated using different rotation speeds in the spin-coater system. However, speeds around 3000-5000 rpm should be applied to have uniform layers along the substrate.

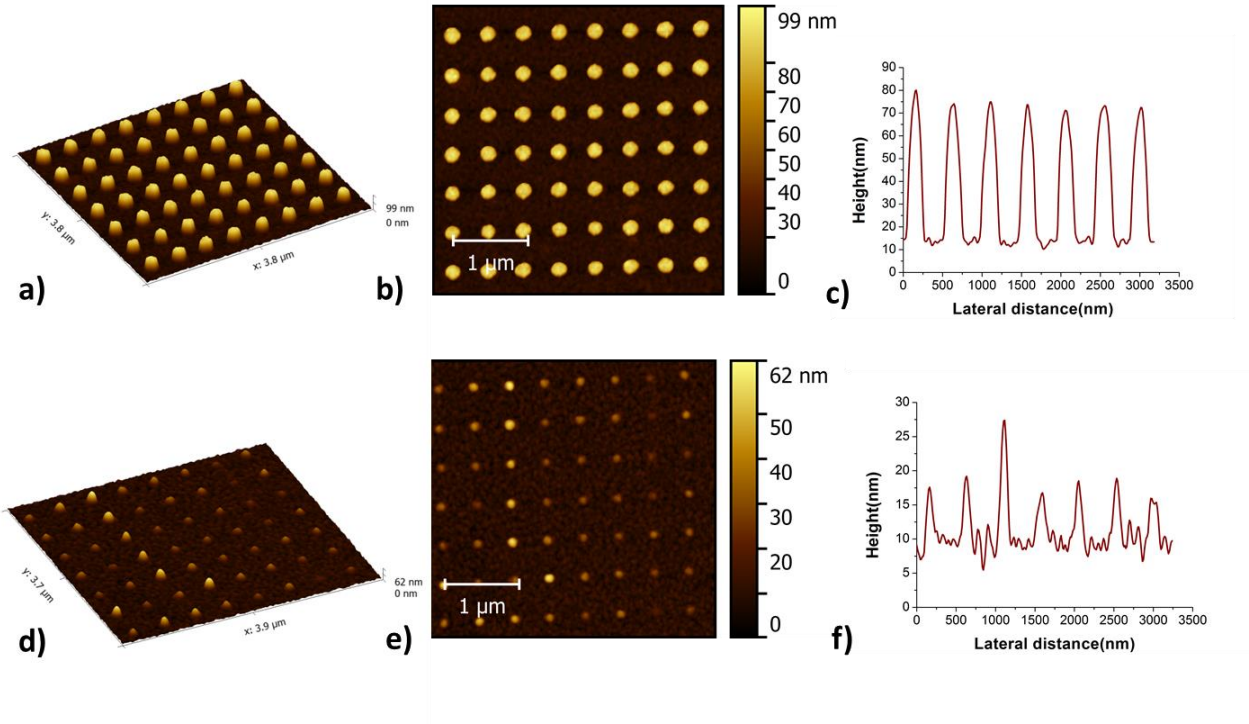

Figure 10. AFM images of the nanoparticles arrays: a) 3D view and b) 2D view after 55s development and c) profile of the particles d) 3D view and e) 2D view after 60s development and f) profile of the particles. Exposition time 3x3 min., 1:2 resist dilution ratio, 1:15 developer dilution ratio.

From Figure 10, we can observe how influential the developing time in our samples is. The nanoparticles arrays exhibit a high aspect ratio after 55 seconds development with a diameter around 200 nm and height about 80 nm. Nonetheless, by increasing just 5 seconds the developing time, the particles are further developed and the diameter is about 100 nm. In summary, for the chosen period Λ=475 nm, the mask can be tuned to feature nanohole arrays with the diameter smaller than 250 nm and steepness of the wall as good as 80 nm. In addition, the can be adopted for fabrication of round nanoparticles with the diameter as small as 100-200 nm and steepness 80-20 nm.

4.3 Photoresists mask templates using MF-26A developer

The change in the developer composition and its subsequent dilution allow us, in principle, to create an undercut profile in the lift off layer, by controlling the etching rate values of this sacrificial layer. Consequently, we need to dilute the developer (1:0.20-1:0.75 dilution ratio) in order to control the process (see 4.1.2). However, the photoresist performance is highly affected by this change and much higher exposition dose is required in order to achieve a defined pattern on the resist. For 1:025 dilution ratio of the developer, a single exposure dose of 230 mJ/cm^2 (12 minutes for 32 µW/cm^2 power) is needed to obtain single gratings with a well-defined aspect ratio as given in Figure 11.

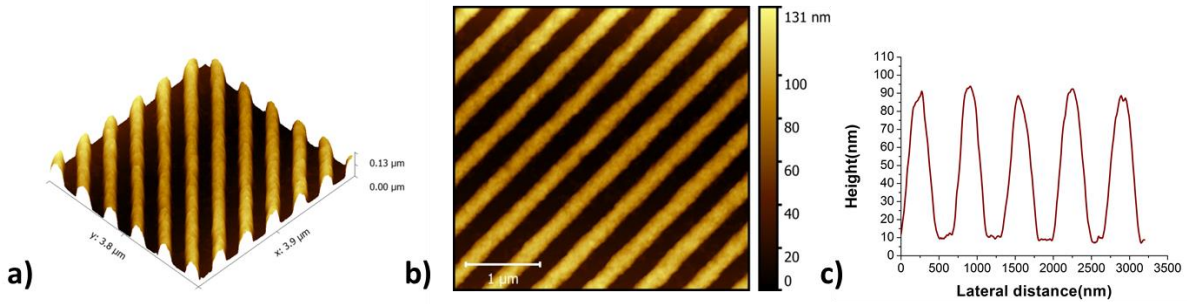

Figure 11. AFM images of single gratings structure: a) 3D view b) 2D view and c) profile of the gratings after 12min exposure and 20s development, 1:0.25 developer dilution ratio, and 1:2 resist dilution ratio.

Applying a second exposure after rotating the sample leads to the desired cross-gratings structures. Nevertheless, after two expositions with an exposition dose between 115-154 mJ/cm^2 each (6-8 minutes each) results in a very rough pattern and without high contrast. The glass substrate is not reached. Besides, the reproducibility of such cross-grating structure is rather difficult.

By increasing the exposition dose further to 192 mJ/cm^2 in each direction (10 min. each), we achieve a well-defined grating, but only in the direction of the first exposition of the interference pattern. However, the other direction after the 90 degree rotation does not exhibit a define pattern as shown in Figure 12. This effect could be caused because the photoresist is overexposed and partially saturated after the first exposure. Thus, it was not possible to obtain cross-grating structures with an equal pattern in both directions by changing the exposition dose equally, developing time and concentration of the developer.

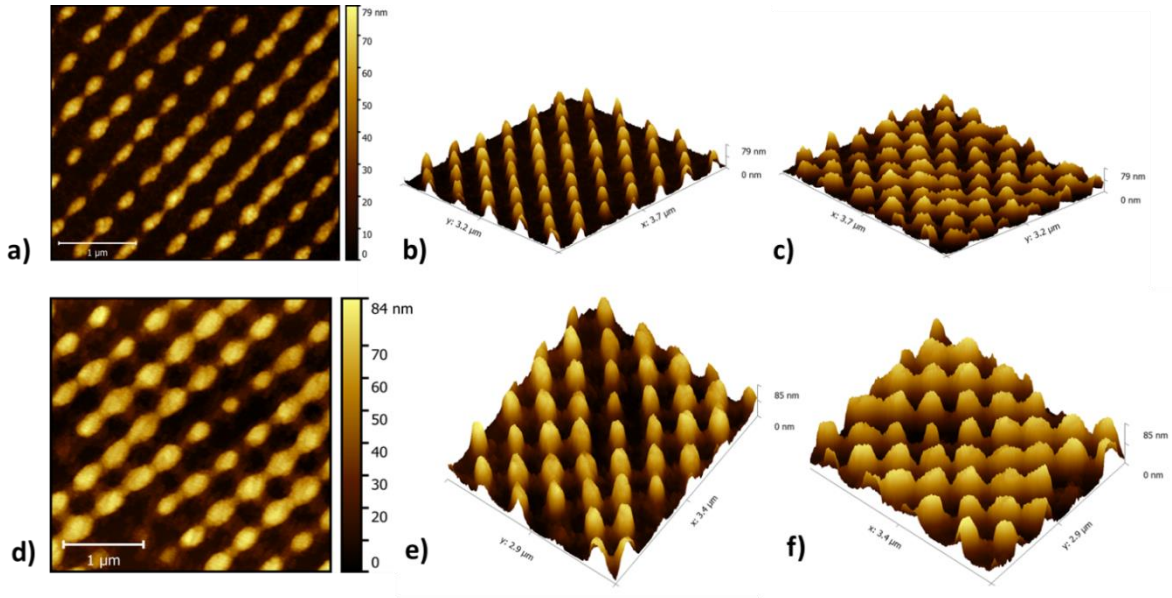

Figure 12. AFM images of nanoparticles array after 10-10 min. double exposure : a) 2D view and b) 3D view of the direction with well-defined aspect ratio c) 3D view of the poor contrast direction by rotating 90 deg. the substrate, for 20s development with 1:0.25 developer ratio; d) 2D view e) 3D view of the direction with well-defined aspect ratio f) 3D view of the poor contrast direction by rotating 90 deg. the sample, for 30s development with 1:0.35 developer ratio.

Trying to compensate this different behavior in the development after exposure, other substrates were evaluated by changing and increasing the second exposition dose of the substrate. These structures are shown in Figure 13. In Figure 13 a) exposition doses of 134 mJ/cm^2 and 163 mJ/cm^2 were employed for first and second exposure respectively. In Figure 13 b) exposition doses of 134 mJ/cm^2 and 154 mJ/cm^2 were carried out.

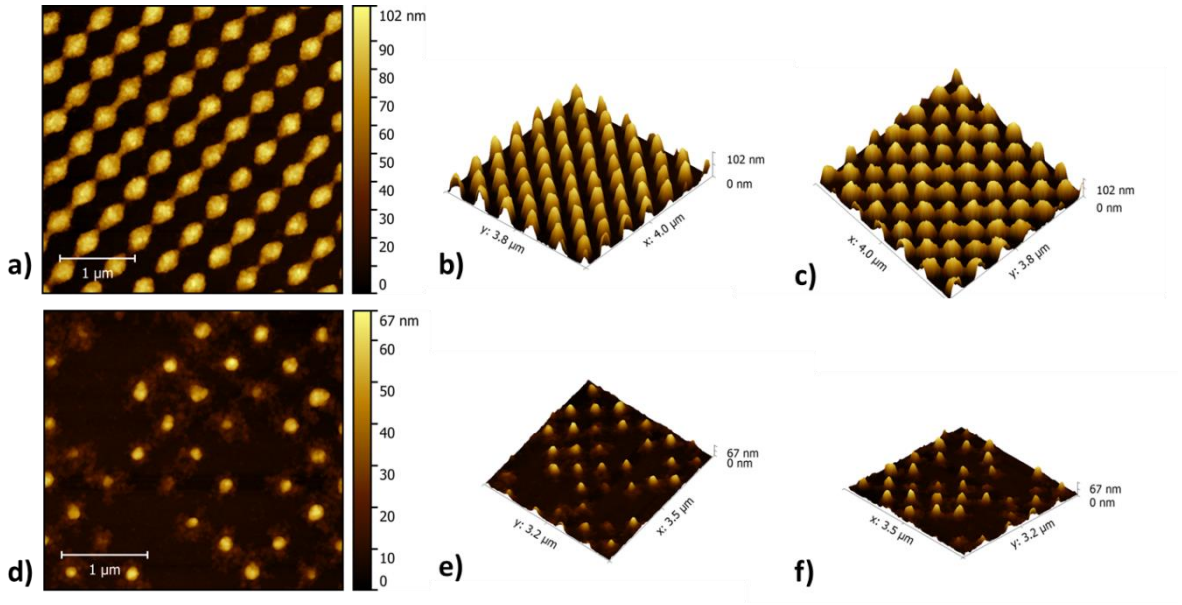

Figure 13. AFM images of the cross-grating structure: a) 2D view and b) c) 3D view of both directions for 7 min and 8.5 min double exposure and 5s development with 1:0.25 dilution ratio; d) 2D view and e) f) 3D view of both directions for 7 and 8 min double exposure and 10s development with 1:0.25 dilution ratio.

In this way we were able to compensate this anisotropy in development and the desired cross-grating pattern can be obtained.

When a higher dilution of the developer is made, 1:0.35 dilution ratio, the nanohole mask template can be produced with high contrast (see Figure 14). Exposition doses of 134 mJ/cm^2 and 163 mJ/cm^2 were employed. The diameter of the holes is around 200 nm.

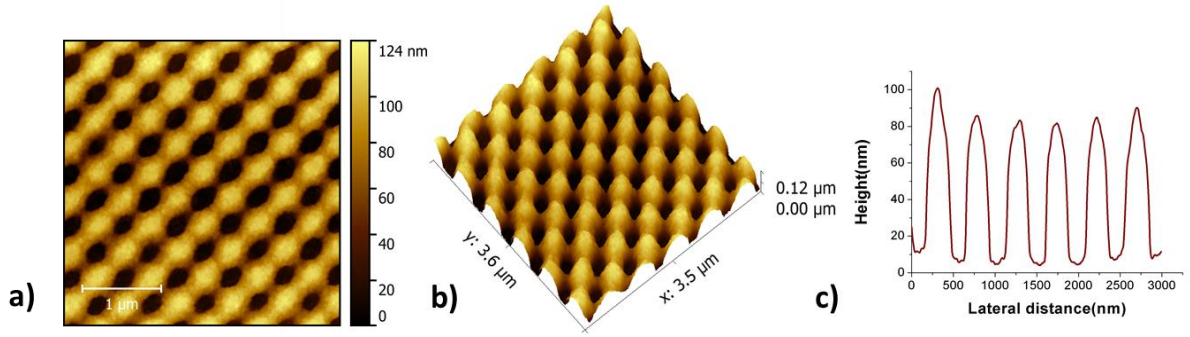

Figure 14. AFM images of the cross-grating structure: a) 2D view and b) 3D view for 7 min and 8.5 min double exposure and 18s development with 1:0.35 dilution ratio.

In summary, the mask can be tuned to feature nanodisk arrays with the diameter between 260-150 nm and steepness of the wall as good as 80-60 nm. The diameter for the mask with the holes is around 200 nm. Theses parameters allow for creating reproducible and well-defined photoresist masks. Then, the undercut layer can be placed and tested underneath the resist.

4.4 Lift off preparation of Au nanoparticle arrays

In principle, a layer structure comprising only a photoresist mask with arrays of nanoholes can be potentially used for preparing the metallic nanoparticle arrays by depositing a metallic layer followed by lift-off. However, this approach was not possible for the prepared masks when a nanoparticle height of *h*=50 nm was targeted. Considering lift-off of the mask by wet etching, the main complication is that the entire nanohole resist template is connected by a thin layer of gold after evaporation and a resist dissolving agent such as acetone cannot penetrate beneath to achieve the lift-off. In order to successfully achieve the lift-off step, the steepness of nanohole walls should be improved. While for dry etching, the photoresist crosslinks on the metallic surface due to the elevate temperatures of the dry etching process and cannot be either removed with the solvent. From temperatures of approx. 150°C onward, all Novolak based resists thermally crosslink and therefore the resist cannot be etched away. The solution that was pursued in this thesis is based on a well-defined undercut profile. This bilayer system enables complete removal of the resist after thermal cross-linking or gold coating.

4.4.1 Approach A - using the mask with nanohole arrays

The nanohole-pattern template can be obtained for the bi-layer system after 35 seconds development with 1:15 AZ-303 developer solution (Figure 15), for two subsequent exposures each with the dose of 57.5 mJ/cm^2. The softbaking temperature was 150°C for 2 min., which is the minimum temperature recommended for the LOR1A polymer,

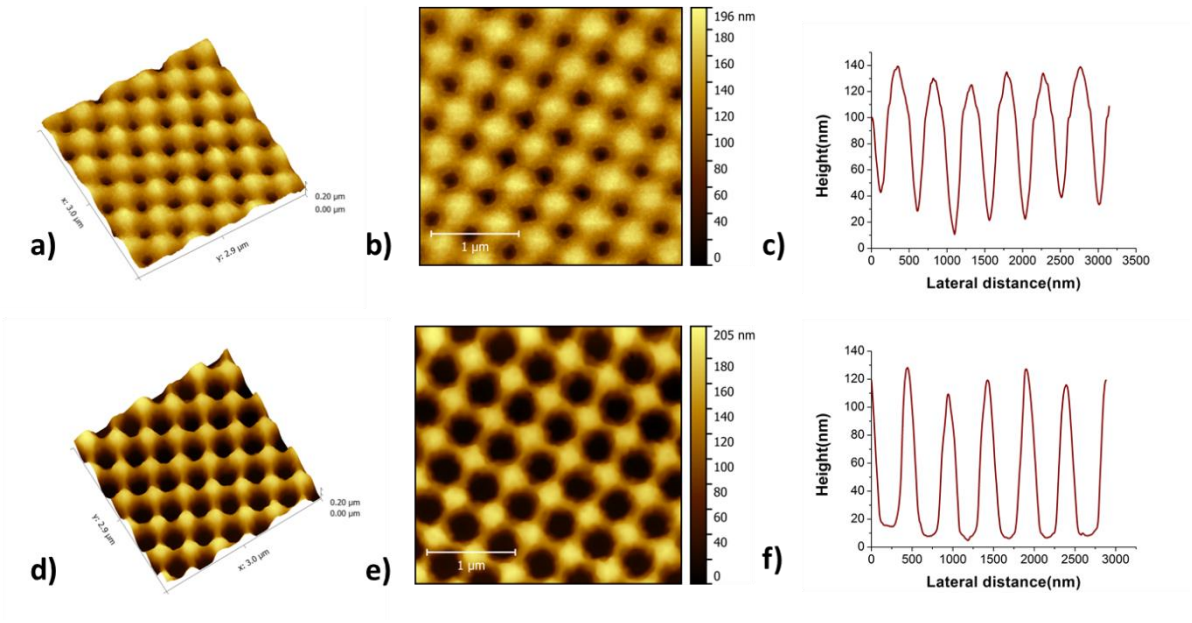

Figure 15. AFM images of nanoholes array with the lift-off layer: a) 3D view and b) 2D view and c) profile of the holes after 35s development and 2 min. softbaking at 150°C for the LOR1A layer; d) 3D view e) 2D view and f) profile of the holes after dry etching.

The etching trough the exposed area, however, does not reach the glass substrate as shown in Figure 15 b). This is a crucial factor since the gold particles created after evaporation would be lift-off if the LOR1A is remaining beneath. When samples are developed more than 35 seconds, the walls separating the holes start to be dissolved. Consequently, the Argon

milling was employed to successfully etch down to the glass substrate. The profile for the holes provides an estimation to detect whether the glass substrate has been reached or not. This flatness at bottom, Figure 15 f), suggests we reached the glass substrate. The lift-off final step after gold evaporation does not succeed completely, because the LOR1A layer is not etched isotropically enough to create the undercut layer. Therefore, the cavities below the S1805 layer (see Figure 6) are not well-created and the entire polymer system is connected by gold. The first lift-off attempt consisted of placing the sample mentioned above in a PG-remover solution stirred at 80°C for 3 hours. On the other hand, the second lift-off attempt was carried out by placing the sample in an ultrasonic bath with PG remover for 20 min. The SEM images of the lift-off process after the evaporation of gold is shown in Figure 16 a) and b).

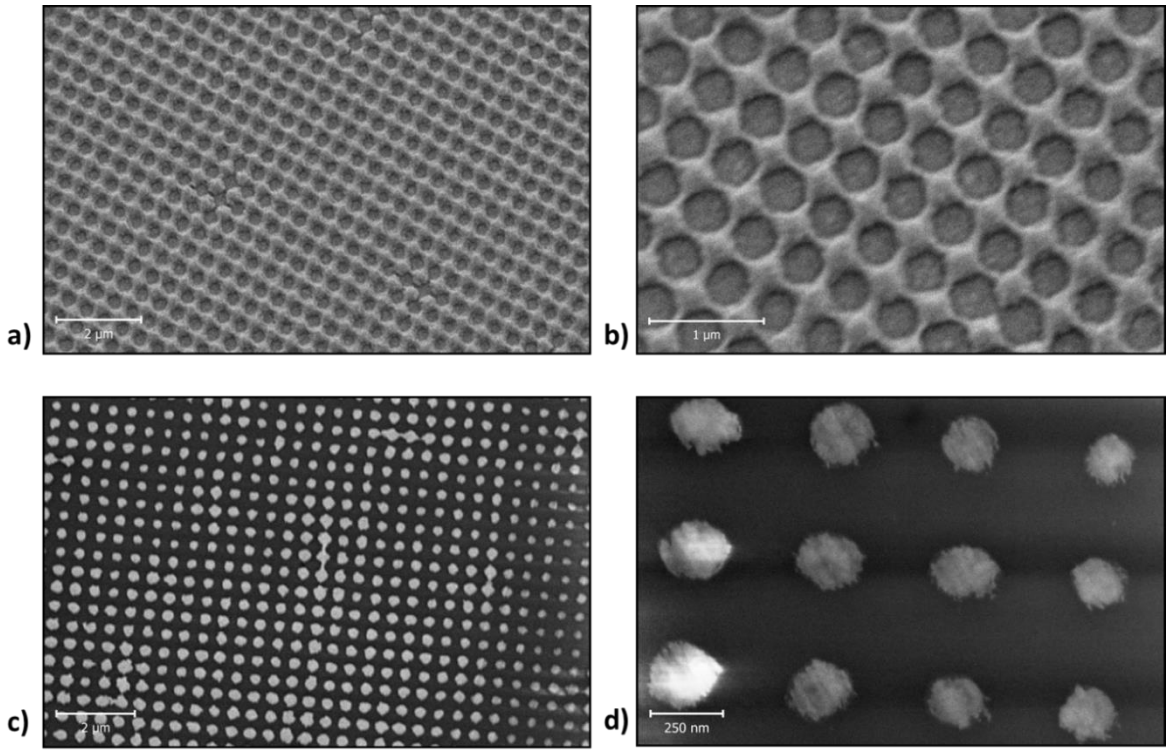

Figure 16. SEM images of the lift off attempt with a) PG remover solution at 80°C; Signal:SE2, EHT=5.00Kv b) Signal:SE2, EHT=5.00Kv, c) Partially lift off after 20 min sonication in PG remover solution Signal:SE2, EHT=3.00Kv d) Signal:SE2, EHT=4.00Kv.

The complete substrate is covered by gold preventing the detachment of the polymers from the surface when the sample is placed in a PG remover solution. By using an ultrasonic bath we were able to speed up the dilution process and obtain the nanoparticles in some areas as shown in Figure 16 c). The diameter of the particles is around 250 nm and the height of the structures is around 50nm. The lift-off process partially works with the sonication but many regions are still partially connected with the polymer layers as shown in Figure 17.

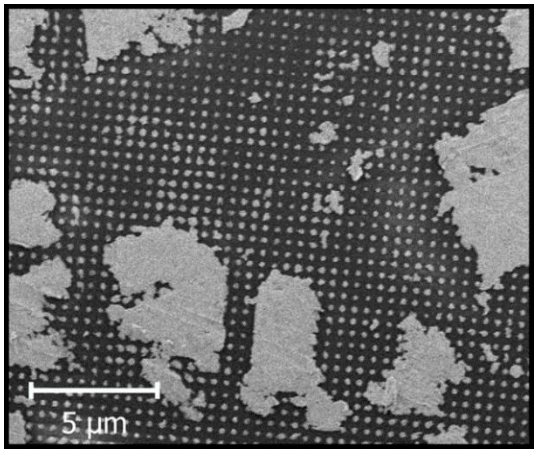

Figure 17. SEM image of the regions connected with the bi-layer system.

Aiming to remove the remaining traces of polymer, the sample was kept several hours under sonication. However, the polymer still remains and the gold particles are washed away.

As observed in section 4.1.1, AZ-303 developer etches faster the resist than the sacrificial layer impeding the undercut formation and the subsequent lift-off is not successful. MF-26A developer, based on TMAH, exhibits the opposite behavior with the suitable etching rates values.

Reproducible nanoholes masks can be obtained with the dilution ratio 1:0.25 of the MF-26A developer and exposition doses of 134 mJ/cm^2 and 163 mJ/cm^2 in the first and second direction respectively. The etching of the sacrificial layer can be adjusted with the softbaking temperature and several experiments were performed baking the LOR1A layer between 150-185°C. For lower baking temperatures (150-160°C) the nanohole mask were formed after 4-6 seconds development. However, the AFM profiles showed that for this developing time the remaining thickness of the LORA layer is still high. If the developing time is increased 1 or 2 seconds the detachment of the bi-layer system was observed. For 170°C temperatures the developing time can be increased to 7-9 seconds and the remaining thickness of the LOR1A is much smaller as shown in Figure 18 and Figure 19.

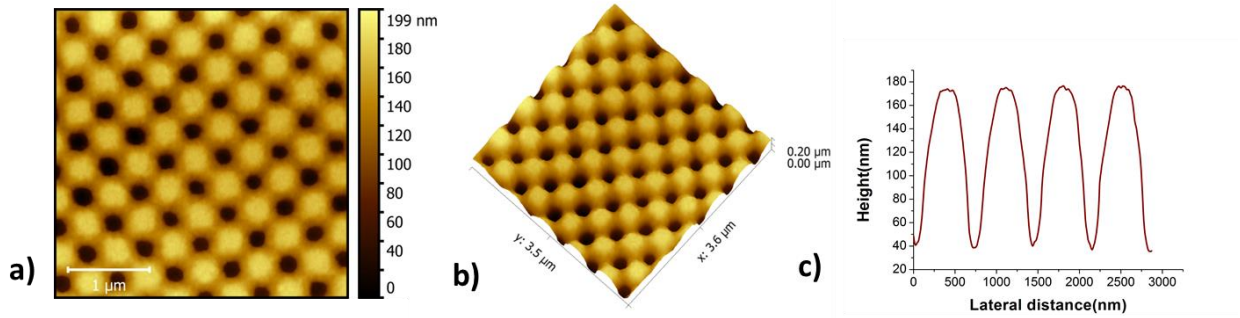

Figure 18. AFM images of nanoholes array with the lift-off layer: a) 3D view and b) 2D view and c) profile of the holes after 7s development and 10 min. softbaking at 170°C for the LOR1A layer.

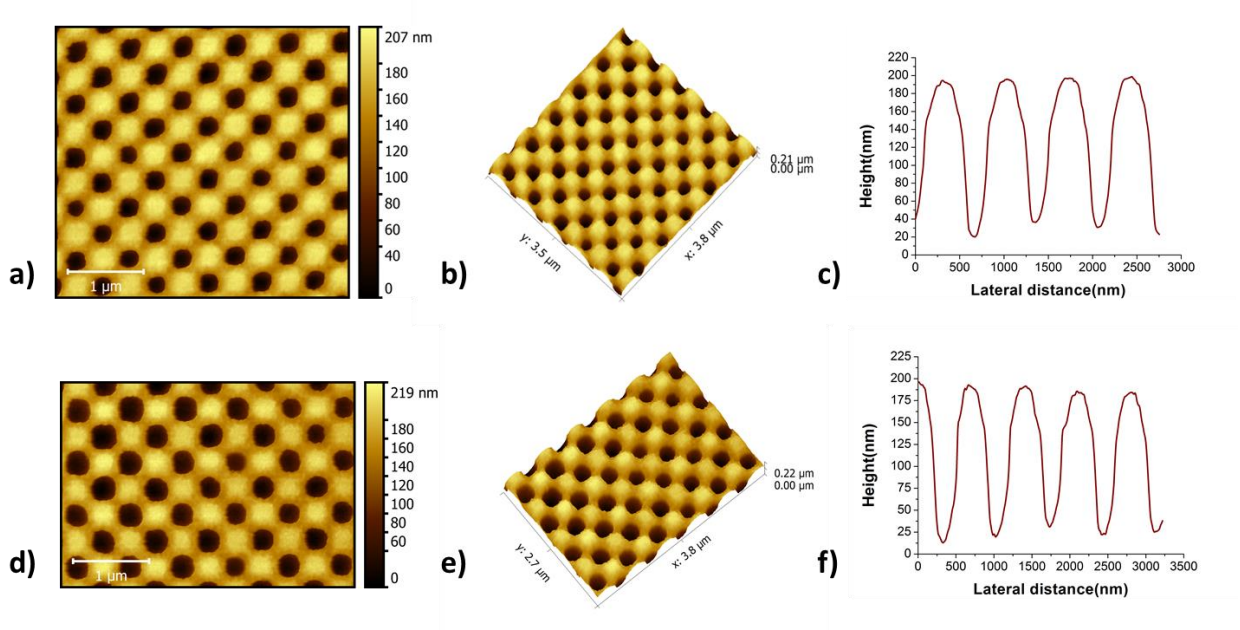

Figure 19. AFM images of nanoholes array with the lift-off layer: a) 3D view and b) 2D view and c) profile of the holes after 8s development and 10 min. softbaking at 170°C for the LOR1A layer; d) 3D view e) 2D view and f) profile of the holes after dry etching with oxygen plasma for 3 min. and 40%power.

Let us notice that by increasing just one second the developing time from 7 s. to 8 s. the height of the holes varies from around 135 nm in Figure 18 c) to 175 nm in Figure 19 c). The high etching rates make complicated to reach the glass substrate without the detachment of the layers. Therefore, a dry etching method is needed to etch to the glass substrate. Plasma etching was used for this purpose as shown in Figure 19 d)-f). Nanoholes masks utilizing 180°C are illustrated in Figure 20. The diameter of the holes is around 200 nm and around 250 nm before and after the dry etching respectively.

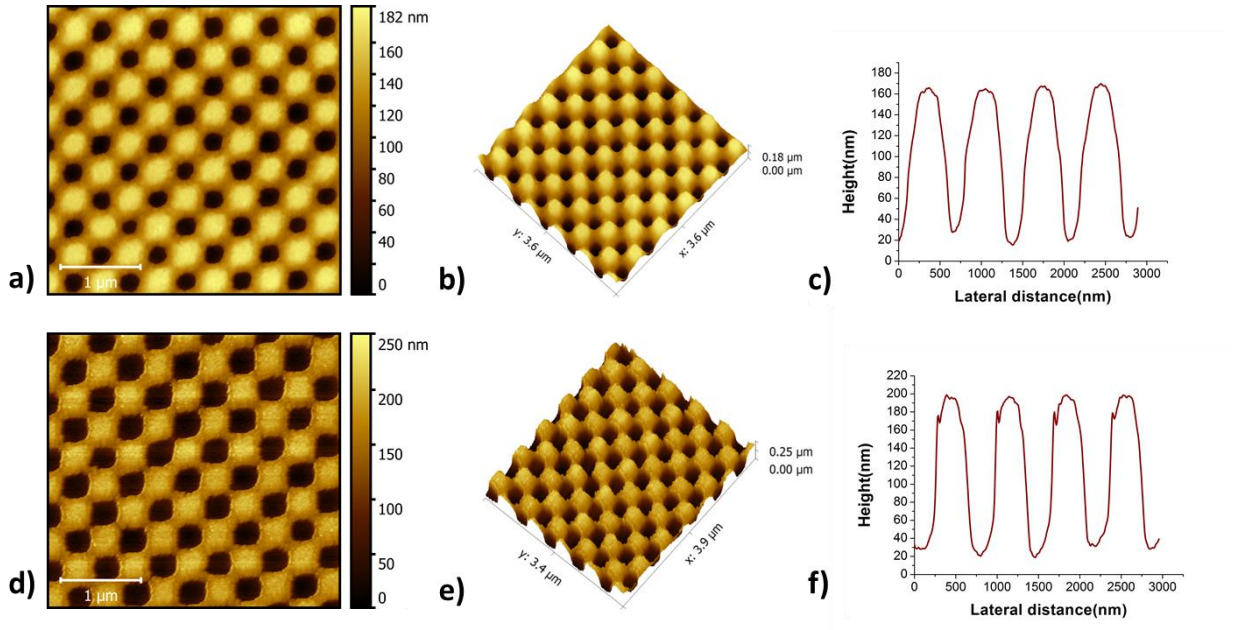

Figure 20. AFM images of nanoholes array with the lift-off layer: a) 3D view and b) 2D view and c) profile of the holes after 10s development and 10 min. softbaking at 180°C for the LOR1A layer; d) 3D view e) 2D view and f) profile of the holes after dry etching with oxygen plasma for 5 min. and 40%power.

Evaporation of gold and lift-off with PG-remover was carried out in the samples mentioned above after dry etching. However, we observed the completely lift-off of the system including the gold particles. This fact suggests that the glass substrate was not reached with the oxygen plasma etching. Therefore, work still needs to be done finding the optimal parameters to etch to the glass substrates with the dry etching while maintaining the contrast of the mask prior evaporation of gold. Let us notice that after 12 seconds development, the walls of the holes in the resist mask are dissolved forming the particles mask. Thus, higher temperatures of 180°C in the softbaking of LOR1A cannot be used to control better the etching rate to the sacrificial layer. Another solution could be to dilute further the concentration of the developer for instance to 1:0.30 ratio aiming to etch further to the glass with wet etching procedure. Some experiments were carried out with 1:0.35 developer ratio but samples lack of contrast and the masks cannot be obtained with the exposition dose provided above. In summary, we showed how to obtain high contrast masks and further experiments could be carried out to reach the glass substrates enabling the fabrication of the metallic particles.

4.4.2 Approach B) - using the mask with nanodisk arrays

Regarding the Approach B) we observed that is not possible to obtain the mask composed of particles arrays using the bi-layer system for the AZ-303 developer. Once the nanoholes are formed the LOR1A starts to be etched and we observed the complete detachment of the layers from the glass surface prior the formation of the particle mask. We believe that smaller thickness of the LOR1A layer (dL) would be needed to avoid lifting up the photoresist nanodisks. Probably if the thickness d_L is much smaller than the diameter of nanoparticles this problem could be solved. AZ-303 developer could be a better option for this approach due to the lower etching rates for the LOR1A layer. If the sacrificial layer is not etched completely to the glass substrate it would not be a major problem following this approach. The Ar milling system etches much faster the LOR1A layer than the resist layer and therefore the mask would remain. Thus, future experiments could be conducted varying the thickness of the sacrificial layer. Regarding the MF-26A developer we obtained the particle mask by using a softbaking temperature of 185°C for the LOR1A layer with the dilution ratio 1:0.25 of the developer and exposition doses of 134 mJ/cm^2 and 163 mJ/cm^2 (see Figure 21).

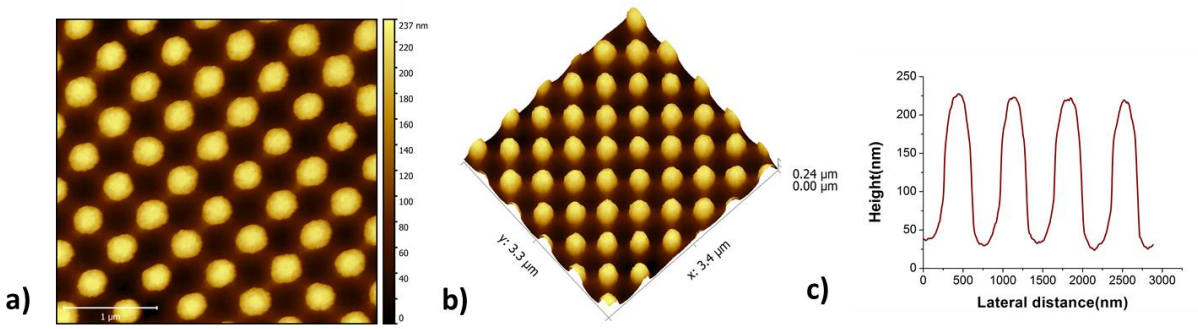

Figure 21. AFM images of nanoparticles array with the lift-off layer: a) 3D view and b) 2D view and c) profile of the particles after 17s development and 5 min. softbaking at 185°C for the LOR1A layer.

The diameter of the particles, however, is limited to 320-380 nm. Higher development times cannot be used without the detachment of the layers from the substrate and to tune particles with lower diameters, the use of the AZ-303 developer is required.

As seen from the results, parameters such as exposition dose, laser wavelength which matches the spectral sensitivity of photoresists, developer type and concentration or resist composition have a great impact in the photoresist performance. The optimization of these elements is essential for obtaining the desired metallic nanostructures. Therefore, establishing a tailor-made and reproducible protocol is crucial in the nanofabrication process. These technological challenges make complex the process and have to be overcome in order to enable the production of such structures. Nevertheless, finding the right values of all these parameters mentioned above is time-consuming since after each single step of the fabrication procedure samples have to be investigated under the microscope. In this work, we provide information about how to obtain high contrast and reproducible photoresist templates with AZ-303 developer, based on sodium hydroxide, and MF-26A, based on tetramethylammonium hydroxide. Nonetheless, a bilayer system is required to obtain metallic structures with wet/dry etching procedures. This AZ-303 developer is not suitable for the wet etching approach with the nanohole mask because a well-defined undercut cannot be created. However, it holds potential for the dry etching approach with the particles mask. On the other hand, the MF-26A developer, based on TMAH, shows great promise for the approach with nanoholes mask but there is still some work to be done particularly optimizing the dry etching parameters. Once these technical issues are solved, such kind of diffractive particle arrays can be fabricated in a symmetric refractive index environment placing silver and a low refractive index layer below the bilayer system.

5. Conclusion

Laser interference lithography was successfully adapted for a preparation of diffractive arrays of Au nanoparticles with the subwavelength dimensions (diameter down to 250 nm and height about 50 nm). A systematic study of using a two layer system that allows for implementing an undercut was carried out and explored for two preparation routes. The first route utilizes dry etching in order to transfer a mask with arrays of polymer disk particles to an underneath metallic film. The preparation of mask with disk diameter as small as 100 nm was achieved. A layer architecture for successful lift-off by using an undercut was suggested. The second route relies on preparing a photoresist mask with arrays of nanoholes followed by a deposition of a thin metal film and lifting off the mask. In combination with undercut, this approach allowed to prepare Au disks with the diameter as small as 250 nm and height 50 nm. For the implementation of these two routes, a two polymer layer system with a photoresist S1805 and undercut layer LOR1A was investigated in detail in terms of controlled etching rates. The presented results can be combined with more sophisticated LIL recording schemes that would allow improve the contrast and thus increase the steepnes and size of prepared mask features such as nanoholes or nanoparticles. This can be in principle achieved by, e.g., recording an interference field with higher contracts which can be achieved by pattern that is formed by simultaneous interference of more than two coherent beams which can be achieved by using special designed mirrors [27] or transmission phase masks [61]. In general, the developed protocols can be adopted for large area preparation of a vast class of plasmonic nanostructures including arrays of nanoholes, spherical nanodisks, nanorods, or nanolines with plasmonic characteristics tailored for specific spectroscopy applications including assays utilizing plasmon-enhanced fluorescence where cost-effect large area structuring is needed in order to establish this amplification scheme in important analytical application areas.

6. References

[1] K. Aslan, I. Gryczynski, J. Malicka, E. Matveeva, J. R. Lakowicz, and C. D. Geddes, "Metal-enhanced fluorescence: An emerging tool in biotechnology," *Curr. Opin. Biotechnol.*, vol. 16, no. 1 SPEC. ISS., pp. 55–62, 2005.

[2] P. Biagioni, J.-S. Huang, and B. Hecht, "Nanoantennas for visible and infrared radiation," vol. 024402, p. 76, 2011.

[3] A. R. L. Caires, L. R. Costa, and J. Fernandes, "A close analysis of metal-enhanced fluorescence of tryptophan induced by silver nanoparticles: wavelength emission dependence," *Cent. Eur. J. Chem.*, vol. 11, no. 1, pp. 111–115, 2013.

[4] C. L. Feng, M. Yin, D. Zhang, S. Zhu, A. M. Caminade, J. P. Majoral, and K. Müllen, "Fluorescent core-shell star polymers based bioassays for ultrasensitive DNA detection by surface plasmon fluorescence spectroscopy," *Macromol. Rapid Commun.*, vol. 32, no. 8, pp. 679–683, 2011.

[5] S. K. Ghosh, D. S. Rahman, A. L. Ali, and A. Kalita, "Surface Plasmon Tunability and Emission Sensitivity of Ultrasmall Fluorescent Copper Nanoclusters," *Plasmonics*, vol. 8, no. 3, pp. 1457–1468, 2013.

[6] R. Gill, L. Tian, W. R. C. Somerville, E. C. Le Ru, and H. Van Amerongen, "Silver Nanoparticle Aggregates as Highly E ffi cient Plasmonic Antennas for Fluorescence Enhancement," 2012.

[7] J. Parsons, E. Hendry, J. R. Sambles, and W. L. Barnes, "Localized surface-plasmon resonances and negative refractive index in nanostructured electromagnetic metamaterials," *Phys. Rev. B - Condens. Matter Mater. Phys.*, vol. 80, no. 24, pp. 1–6, 2009.

[8] K. Toma, J. Dostalek, and W. Knoll, "Fluorescence Emission for Biosensor Applications," vol. 19, no. 12, pp. 97–106, 2011.

[9] P. Genevet, J. P. Tetienne, E. Gatzogiannis, R. Blanchard, M. a. Kats, M. O. Scully, and F. Capasso, "Large enhancement of nonlinear optical phenomena by plasmonic nanocavity gratings," *Nano Lett.*, vol. 10, no. 12, pp. 4880–4883, 2010.

[10] P. K. Jain, K. S. Lee, I. H. El-Sayed, and M. a. El-Sayed, "Calculated absorption and scattering properties of gold nanoparticles of different size, shape, and composition: Applications in biological imaging and biomedicine," *J. Phys. Chem. B*, vol. 110, no. 14, pp. 7238–7248, 2006.

[11] A. M. Kern and O. J. F. Martin, "Excitation and reemission of molecules near realistic plasmonic nanostructures," *Nano Lett.*, vol. 11, no. 2, pp. 482–487, 2011.

[12] D. Punj, M. Mivelle, S. B. Moparthi, T. S. van Zanten, H. Rigneault, N. F. van Hulst, M. F. García-Parajó, and J. Wenger, "A plasmonic 'antenna-in-box' platform for enhanced single-molecule analysis at micromolar concentrations.," *Nat. Nanotechnol.*, vol. 8, no. 7, pp. 512–6, 2013.

[13] A. Kinkhabwala, Z. Yu, S. Fan, Y. Avlasevich, K. Müllen, and W. E. Moerner, "Large single-molecule fluorescence enhancements produced by a bowtie nanoantenna," *Nat. Photonics*, vol. 3, no. 11, pp. 654–657, 2009.

[14] M. Bauch and J. Dostalek, "Collective localized surface plasmons for high performance fluorescence biosensing," *Opt. Express*, vol. 21, no. 17, pp. 637–644, 2013.

[15] S. Panaro, a. Toma, R. P. Zaccaria, M. Chirumamilla, a. Saeed, L. Razzari, G. Das, C. Liberale, F. De Angelis, and E. Di Fabrizio, "Design and top-down fabrication of metallic L-shape gap nanoantennas supporting plasmon-polariton modes," *Microelectron. Eng.*, vol. 111, pp. 91–95, 2013.

[16] M. Grande, G. V. Bianco, M. a. Vincenti, D. De Ceglia, V. Petruzzelli, M. Scalora, G. Bruno, a. D'Orazio, M. De Vittorio, and T. Stomeo, "2D plasmonic gold nano-patches for linear and nonlinear applications," *Microelectron. Eng.*, vol. 111, pp. 234–237, 2013.
[17] N. Kalhor, S. a. Boden, and H. Mizuta, "Sub-10 nm patterning by focused He-ion beam milling for fabrication of downscaled graphene nano devices," *Microelectron. Eng.*, vol. 114, pp. 70–77, 2014.
[18] H. Lim, K. B. Choi, G. Kim, S. Lee, H. Park, J. Ryu, S. Jung, and J. Lee, "Roll-to-roll nanoimprint lithography for patterning on a large-area substrate roll," *Microelectron. Eng.*, vol. 123, pp. 18–22, 2014.
[19] H. Yoshikawa, J. Taniguchi, G. Tazaki, and T. Zento, "Fabrication of high-aspect-ratio pattern via high throughput roll-to-roll ultraviolet nanoimprint lithography," *Microelectron. Eng.*, vol. 112, pp. 273–277, 2013.
[20] J. C. Hulteen, "Nanosphere lithography: A materials general fabrication process for periodic particle array surfaces," *J. Vac. Sci. Technol. A Vacuum, Surfaces, Film.*, vol. 13, no. 3, p. 1553, 1995.
[21] F. Xie, A. Centeno, M. R. Ryan, D. J. Riley, and N. M. Alford, "Au nanostructures by colloidal lithography: from quenching to extensive fluorescence enhancement," *J. Mater. Chem. B*, vol. 1, no. 4, p. 536, 2013.
[22] A. Rodriguez, M. Echeverría, M. Ellman, N. Perez, Y. K. Verevkin, C. S. Peng, T. Berthou, Z. Wang, I. Ayerdi, J. Savall, and S. M. Olaizola, "Laser interference lithography for nanoscale structuring of materials: From laboratory to industry," *Microelectron. Eng.*, vol. 86, no. 4–6, pp. 937–940, 2009.
[23] M. Bauch, S. Hageneder, and J. Dostalek, "Plasmonic amplification for bioassays with epi- fluorescence readout," vol. 9, no. 4, 2014.
[24] H. Liu, X. Zhang, and T. Zhai, "Plasmonic nano-ring arrays through patterning gold nanoparticles into interferograms.," *Opt. Express*, vol. 21, no. 13, pp. 15314–22, 2013.
[25] C. H. Liu, M. H. Hong, H. W. Cheung, F. Zhang, Z. Q. Huang, L. S. Tan, and T. S. a Hor, "Bimetallic structure fabricated by laser interference lithography for tuning surface plasmon resonance.," *Opt. Express*, vol. 16, no. 14, pp. 10701–10709, 2008.
[26] F. Y. Lee, K. H. Fung, T. L. Tang, W. Y. Tam, and C. T. Chan, "Fabrication of gold nano-particle arrays using two-dimensional templates from holographic lithography," *Curr. Appl. Phys.*, vol. 9, no. 4, pp. 820–825, 2009.
[27] M. Vala and J. Homola, "Flexible method based on four-beam interference lithography for fabrication of large areas of perfectly periodic plasmonic arrays," *Opt. Express*, vol. 22, no. 15, p. 18778, 2014.
[28] B. Van Dorst, J. Mehta, K. Bekaert, E. Rouah-Martin, W. De Coen, P. Dubruel, R. Blust, and J. Robbens, "Recent advances in recognition elements of food and environmental biosensors: A review," *Biosens. Bioelectron.*, vol. 26, no. 4, pp. 1178–1194, 2010.
[29] T. Ahuja, I. A. Mir, D. Kumar, and Rajesh, "Biomolecular immobilization on conducting polymers for biosensing applications," *Biomaterials*, vol. 28, no. 5, pp. 791–805, 2007.
[30] L. Su, W. Jia, C. Hou, and Y. Lei, "Microbial biosensors: A review," *Biosens. Bioelectron.*, vol. 26, no. 5, pp. 1788–1799, 2011.
[31] S. Mross, S. Pierrat, T. Zimmermann, and M. Kraft, "Microfluidic enzymatic biosensing systems: A review," *Biosens. Bioelectron.*, vol. 70, pp. 376–391, 2015.
[32] D. Dey and T. Goswami, "Optical biosensors: A revolution towards quantum nanoscale electronics device fabrication," *J. Biomed. Biotechnol.*, vol. 2011, 2011.

[33] M. N. Velasco-Garcia, “Optical biosensors for probing at the cellular level: A review of recent progress and future prospects,” *Semin. Cell Dev. Biol.*, vol. 20, no. 1, pp. 27–33, 2009.
[34] C. R. Taitt, G. P. Anderson, and F. S. Ligler, “Evanescent wave fluorescence biosensors,” *Biosens. Bioelectron.*, vol. 20, no. 12, pp. 2470–2487, 2005.
[35] J. Cao, T. Sun, and K. T. V Grattan, “Gold nanorod-based localized surface plasmon resonance biosensors: A review,” *Sensors Actuators, B Chem.*, vol. 195, pp. 332–351, 2014.
[36] E. Petryayeva and U. J. Krull, “Localized surface plasmon resonance: Nanostructures, bioassays and biosensing-A review,” *Anal. Chim. Acta*, vol. 706, no. 1, pp. 8–24, 2011.
[37] P. Petrou, I. Raptis, S. Kakabakos, T. Speliotis, a. Gerardino, and N. Papanikolaou, “Fluorescence enhancement from plasmonic Au templates,” *Microelectron. Eng.*, vol. 88, no. 8, pp. 1845–1848, 2011.
[38] R. Osgood, L. Cao, N. Panoiu, W. Fan, S. Zhang, K. Malloy, and S. Brueck, “Nonlinear Plasmonics,” vol. 6, no. October, pp. 737–748, 2009.
[39] C. Boozer, G. Kim, S. Cong, H. Guan, and T. Londergan, “Looking towards label-free biomolecular interaction analysis in a high-throughput format: a review of new surface plasmon resonance technologies,” *Curr. Opin. Biotechnol.*, vol. 17, no. 4, pp. 400–405, 2006.
[40] J. Homola, S. S. Yee, and G. Gauglitz, “Surface plasmon resonance sensors: review,” *Sensors Actuators B Chem.*, vol. 54, no. 1–2, pp. 3–15, 1999.
[41] A. Abbas, M. J. Linman, and Q. Cheng, “New trends in instrumental design for surface plasmon resonance-based biosensors,” *Biosens. Bioelectron.*, vol. 26, no. 5, pp. 1815–1824, 2011.
[42] Y. Wang, A. Brunsen, U. Jonas, J. Dostálek, and W. Knoll, “Prostate specific antigen biosensor based on long range surface plasmon-enhanced fluorescence spectroscopy and dextran hydrogel binding matrix,” *Anal. Chem.*, vol. 81, no. 23, pp. 9625–9632, 2009.
[43] Y. Jiang, H. Wang, H. Wang, B. Gao, Y. Hao, Y. Jin, Q. Chen, and H. Sun, “Surface Plasmon Enhanced Fluorescence of Dye Molecules on Metal,” *Science (80-.).*, pp. 12636–12642, 2011.
[44] J. R. Lakowicz, Y. Shen, S. D’Auria, J. Malicka, J. Fang, Z. Gryczynski, and I. Gryczynski, “Radiative decay engineering. 2. Effects of Silver Island films on fluorescence intensity, lifetimes, and resonance energy transfer.,” *Anal. Biochem.*, vol. 301, no. 2, pp. 261–277, 2002.
[45] C. W. Blackledge, T. Tabarin, E. Masson, R. J. Forster, and T. E. Keyes, “Silica nanoparticles containing a rhodamine dye and multiple gold nanorods,” *J. Nanoparticle Res.*, vol. 13, no. 10, pp. 4659–4672, 2011.
[46] S.-H. Cao, W.-P. Cai, Q. Liu, and Y.-Q. Li, “Surface Plasmon–Coupled Emission: What Can Directional Fluorescence Bring to the Analytical Sciences?,” *Annu. Rev. Anal. Chem.*, vol. 5, no. 1, pp. 317–336, 2012.
[47] M. Bauch, K. Toma, M. Toma, Q. Zhang, and J. Dostalek, “Plasmon-Enhanced Fluorescence Biosensors: a Review,” *Plasmonics*, pp. 1–19, 2013.
[48] O. Stranik, H. M. McEvoy, C. McDonagh, and B. D. MacCraith, “Plasmonic enhancement of fluorescence for sensor applications,” *Sensors Actuators, B Chem.*, vol. 107, no. 1 SPEC. ISS., pp. 148–153, 2005.

[49] J. W. Liaw, H. Y. Tsai, and C. H. Huang, “Size-Dependent Surface Enhanced Fluorescence of Gold Nanorod: Enhancement or Quenching,” *Plasmonics*, vol. 7, no. 3, pp. 543–553, 2012.
[50] I. Kocakarin and K. Yegin, “Surface plasmon-enhanced nanoantenna for localized fluorescence,” *Int. J. Antennas Propag.*, vol. 2012, 2012.
[51] B. Auguié and W. L. Barnes, “Diffractive coupling in gold nanoparticle arrays and the effect of disorder.,” *Opt. Lett.*, vol. 34, no. 4, pp. 401–403, 2009.
[52] B. Auguié, X. M. Bendaña, W. L. Barnes, and F. J. García De Abajo, “Diffractive arrays of gold nanoparticles near an interface: Critical role of the substrate,” *Phys. Rev. B - Condens. Matter Mater. Phys.*, vol. 82, no. 15, pp. 1–7, 2010.
[53] G. Vecchi, V. Giannini, and J. Gómez Rivas, “Shaping the fluorescent emission by lattice resonances in plasmonic crystals of nanoantennas,” *Phys. Rev. Lett.*, vol. 102, no. 14, pp. 1–11, 2009.
[54] M. Bauch, “New enhancement strategies for plasmon-enhanced fluorescence biosensors,” 2014.
[55] P. Rodríguez-Franco, a. Arriola, N. Darwish, J. J. Jaramillo, H. Keshmiri, T. Tavera, S. M. Olaizola, and M. Moreno, “Fabrication of broad area optical nanostructures for high throughput chemical sensing,” *Sensors Actuators, B Chem.*, vol. 187, pp. 356–362, 2013.
[56] H. Wolferen, L. Abelmann, and H. van Wolferen, “Laser interference lithography,” *Lithogr. Princ. Process. Mater.*, pp. 133–148, 2011.
[57] J. Park, W. Leung, K. Constant, S. Chaudhary, T. Kim, and K. Ho, “Laser Interference Lithography for Fabricating Nanowires and Nanoribbons,” *Nanowires - Implementations Appl.*, vol. 1, 2011.
[58] R. B. Darling, “EE-527 : MicroFabrication Positive Photoresists.” [Online]. Available: www.ee.washington.edu/research/microtech/cam/PROCESSES/positivephotoresistpdf.html.
[59] A. Reiser, J. P. Huang, X. He, T. F. Yeh, S. Jha, H. Y. Shih, M. S. Kim, Y. K. Han, and K. Yan, “The molecular mechanism of novolak-diazonaphthoquinone resists,” *Eur. Polym. J.*, vol. 38, no. 4, pp. 619–629, 2002.
[60] M. L. Long and J. Newmann, “Image reversal techniques with standard positive photoresist,” *SPIE Proc. Vol. 469 Adv. Resist Technol.*, vol. 469, pp. 189–193, 1984.
[61] S. Lattice and P. Generation, “2D Phase masks.” [Online]. Available: http://www.ibsenphotonics.com/wp-content/uploads/Ibsen-Product-Sheet-2D-Phase-masks.pdf.